Supplemental Material
Structural nonequilibrium forces in driven colloidal systems

Nico C. X. Stuhlmüller,[1] Tobias Eckert,[1] Daniel de las Heras,[1] and Matthias Schmidt[1]
[1] *Theoretische Physik II, Physikalisches Institut, Universität Bayreuth, D-95440 Bayreuth, Germany*

Superadiabatic force profiles under strong driving conditions

The examples presented in the main text address the behaviour of the system in response to relatively weak external perturbations. Here we show that under strong external driving conditions, both superadiabatic force profiles change significantly. We show in Supplemental Fig. 1 the viscous and the structural superadiabatic forces for both weak and for strong external driving conditions. We find that the direction of both force fields remains unchanged upon increasing the driving. Hence, for the cases considered here, the viscous force opposes always the external force and the structural force sustains (counteracts) the density gradient. However, although the only difference between both driving conditions is the magnitude of the external driving, the superadiabatic (position-dependent) force profiles change significantly their shape depending on the strength of the driving. The power functional approximation presented in Eq. (15) of the main text is intended to deal with low/moderate driving and does not fully reproduce the characteristics of the superadiabatic forces at high driving conditions. Note that the magnitude of the superadiabatic force is relatively small as compared to the magnitude of the external force, even for the case of weak driving (Fig. 1 of the main text). Therefore, the velocity field basically follows the external driving, and the superadiabatic forces are then given by Eq. (18) of the main text. That is, the theory does not reproduce the shape change of the superadiabatic forces with the magnitude of the external driving (Supplemental Fig. 1). This was expected since in Eq. (15) we have only incorporated the first two terms of the expansion of $P_t^{\rm exc}$ in powers of $\nabla\mathbf{v}$. Therefore, one expects Eq. (15) to be valid under weak driving conditions. The correct treatment of strong driving conditions requires the addition of higher order terms to Eq. (15). It is straightforward to incorporate such terms by rewriting the excess superadiabatic functional as

$$P^{\rm exc} = \int d\mathbf{r}\Big[\eta(\nabla\times\mathbf{v})^2 - \chi(\nabla\cdot\mathbf{v})(\nabla\times\mathbf{v})^2\Big]h(\nabla\mathbf{v}), \quad (1)$$

where $h(\nabla\mathbf{v})$ is a scalar-valued function, which we choose to have the following form:

$$h(\nabla\mathbf{v}) = \frac{1}{1+c_0(\nabla\times\mathbf{v})^2}, \quad (2)$$

where c_0 is a positive constant which controls the strength of the influence of the flow; setting $c_0 = 0$ recovers the form of Eq. (15) of the main text. In Eq. (1) we have assumed steady state conditions and therefore eliminated the time integrals. The first two terms of a series expansion of Eq. (1) in $\nabla\mathbf{v}$ have the same functional structure as that presented in Eq. (15) of the main text. In addition, Eq. (1) incorporates higher order contributions in $\nabla\mathbf{v}$. We find that the superadiabatic force profile that result upon functional differentiation of Eq. (1) is in excellent agreement with the simulation results both for weak and for strong driving conditions (see black circles in Supplemental Fig. 1). For both cases shown in the figure, we have set $c_0 = 3.5\cdot10^{-3}\ \tau^2$ and fit the values of η and χ. The values of η and of χ determine the overall amplitude of the viscous and of the structural superadiabatic force, respectively. We find that the values of η and χ seem to depend on the magnitude of the external driving, which is a clear indication that Eq. (1) constitutes only a first approximation.

Scaling of the superadiabatic forces with the inverse box length

We present a scaling analysis of the magnitude of the viscous and of the structural superadiabatic force fields with the amplitude of the external driving and the overall density in the main text. Here, we focus on the scaling of these force fields with the wavenumber $k = 2\pi/L$ that characterizes the inhomogeneous shear profile, cf. Eq. (9) of the main text. In practice we change k by changing the box size L, ensuring that the other relevant variables are unchanged, e.g. keeping the mean density constant by accordingly modifying the number of particles, N.

Our theory, cf. Eq. (18) of the main text, predicts different types of scaling with k for the viscous (quadratic in k) and for the structural (cubic in k) superadiabatic forces. We fix the amplitude of the external driving ($f_0 \approx 0.30\epsilon/\sigma$) and the average density of the system ($\rho_0\sigma^2 = 0.02$). Therefore, according to Eq. (18) of the main text, the only remaining dependence of the amplitude of the superadiabatic forces is on k. In Supplemental Fig. 2 we show the amplitude of the superadiabatic forces as a function of the wavenumber. The smallest system corresponds to $N = 2$ and $H/\sigma = 10$, and the largest one to $N = 100$ and $H/\sigma = 70.7$. Each curve shows three different regimes. For small boxes (large wavenumber) we observe a saturation of the superadiabatic forces, sim-

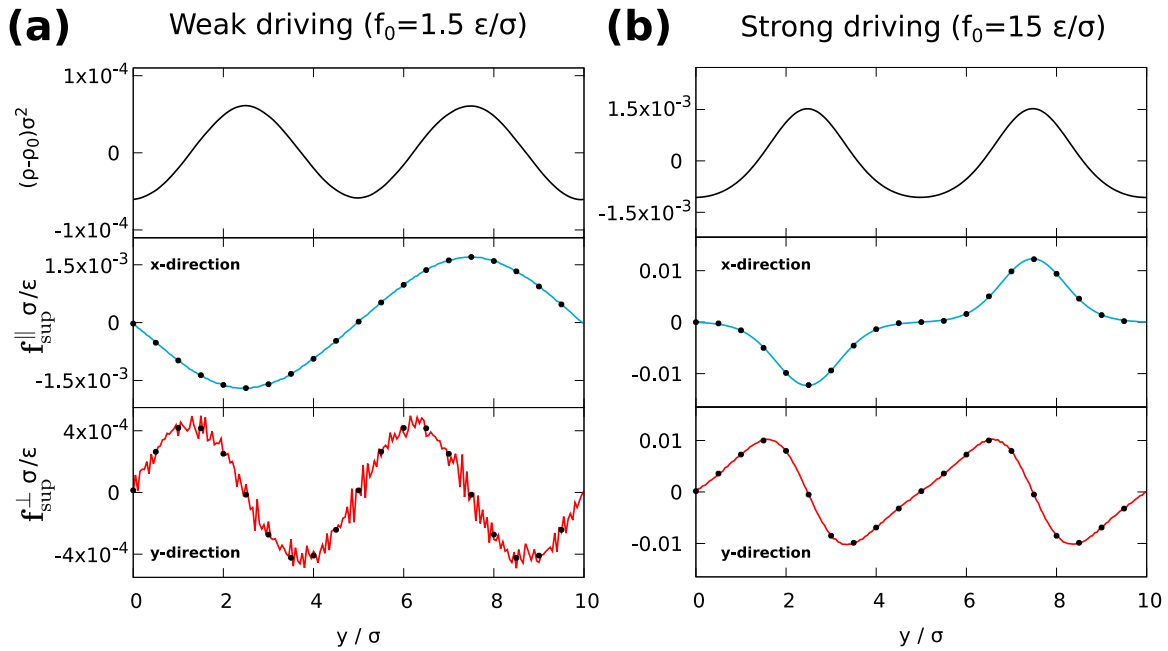

Supplemental Fig. 1. Steady-state density and force profiles according to BD simulations in a system with $N = 25$, $L/\sigma = 10$, and $k_BT/\epsilon = 1.0$. Results are shown for two strengths of the external driving force: (a) $f_0 \approx 1.5\epsilon/\sigma$, weak external driving, and (b) $f_0 \approx 15\epsilon/\sigma$, strong external driving. (Top panels) Density profile, measured from the average density $\rho_0 = N/L^2 = 0.25\sigma^{-2}$, as a function of y. (Middle panel) Superadiabatic viscous force acting along $\mathbf{e}_x$ as a function of y obtained by BD simulations (solid-blue line) and theoretically (black circles). (Bottom panel) Superadiabatic structural force acting along $\mathbf{e}_y$ as a function of y obtained by BD simulations (solid-red line) and theoretically (black circles).

ilar to the saturation effect observed by increasing the external driving or the density (see Fig. 2 of the main text). At intermediate wavenumbers the forces scale linearly with k. Finally, for long boxes (small wavenumbers) the curves depart significantly from a linear behaviour. Note that both curves must pass through the origin of coordinates. The low driving conditions that are implicit in going to small values of k render the analysis of the data difficult. Nevertheless, the scaling of the viscous force is fully consistent with the quadratic prediction of the theory, Eq. (18) of the main text. Also, it is evident from the data that the structural force is not linear in k for sufficiently large boxes (small wavenumbers). The precision of our data, however, does not allow us to confirm the cubic scaling predicted by the theory, although the data is also clearly not in contradiction to the analytical result. We hence cannot rule out the contribution of further terms to $P_t^{\rm exc}$. In particular, a term involving the combination $(\nabla\cdot\mathbf{v})(\mathbf{v}\cdot\mathbf{v})$ produces a structural force with the same shape, but a linear scaling with k. We conclude that revealing the true scaling of the superadiabatic forces is a major challenge. Due to the saturation effect, the forces increase linearly in a broad range of system sizes. Only for very small perturbations (very large system sizes in this case) the true scaling behaviour is revealed.

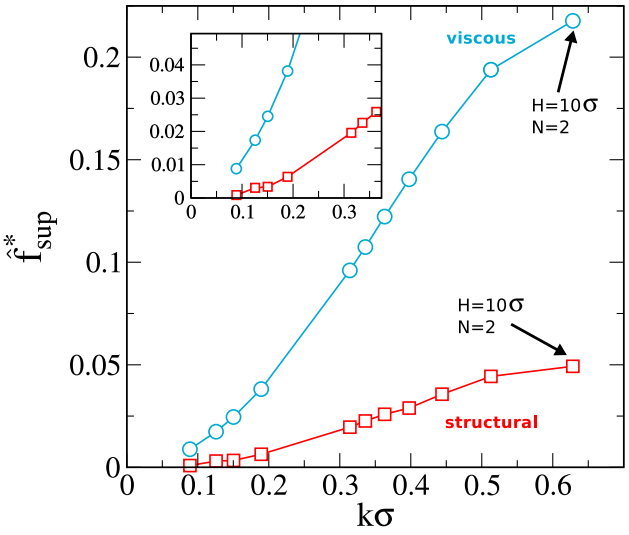

Supplemental Fig. 2. Scaled amplitude of the superadiabatic forces $\hat{f}^*_{\rm sup} = 10^3\hat{f}_{\rm sup}\sigma/\epsilon$ as a function of the (scaled) wavenumber $k\sigma = 2\pi\sigma/L$. The blue circles (red squares) correspond to the viscous (structural) superadiabatic force, as indicated. The lines are guides to the eye. Data obtained with BD simulations for systems with $k_BT/\epsilon = 0.4$ and $f_0 \approx 0.30\epsilon/\sigma$. The number of particles and the length of the box vary across the data points, such that the average density $\rho_0\sigma^2 = 0.02$ is kept constant. Both curves must pass through the origin.

Representation of numerical results via fit functions

The fit parameters in Fig. 2a of the main text are: $A_1 = 3.7 \cdot 10^{-4}$ (for the viscous force, linear in velocity), $A_2 = 3.0 \cdot 10^{-5}\sigma/\epsilon$ (for the structural force, quadratic in velocity). The fit has been done in the region of weak driving $f_0\sigma/\epsilon \lesssim 0.3$.

Regarding the scaling of the superadiabatic forces with the total density, Fig. 2b of the main text ($f_0 \approx 3.14\epsilon/\sigma$), a good numerical representation in the range $0 < \rho_0\sigma^2 < 0.1$ is given by $\eta(\rho_0) \approx 1.7 \cdot 10^{-2}\rho_0^2\epsilon\tau\sigma^2$ and $\chi(\rho_0) \approx 10^{-2}\rho_0^2\epsilon\tau^2\sigma^2 - 0.4 \cdot 10^{-2}\rho_0^3\epsilon\tau^2\sigma^4$.

We reemphasize that the true scaling of viscous and structural forces is only revealed at weak driving conditions and low densities. At intermediate driving and/or total density both forces are linear in velocity and total density due to a, yet to be investigated, saturation mechanism of the superadiabatic forces.

Predicting the density profile

We can obtain a prediction of the density profile from the theory, by projecting the force balance equation (Eq. (1) of the main text) onto $\mathbf{e}_y$ and observing that $\mathbf{v} \cdot \mathbf{e}_y = 0 = \mathbf{f}_{\text{ext}} \cdot \mathbf{e}_y$. We obtain $k_BT\partial\rho/\partial y = f_{\text{sup,y}}$ upon neglecting the adiabatic excess contribution $\mathbf{f}_{\text{adx}}$, as this is small against the ideal term, $|\mathbf{f}_{\text{adx}}| \ll |k_BT\nabla\rho|$ in the low density case $N = 2$. Integrating in y gives to lowest order in the difference $\rho - \rho_0$ the result $\rho(y) = \rho_0 - f_0^2\chi k^2\cos(2ky)/(2\gamma k_BT)$, which describes the low-density case (Fig. 1b of the main text) quite well.